Weather and Climate Extremes 30 (2020) 100289

Contents lists available at ScienceDirect

Weather and Climate Extremes

journal homepage: http://www.elsevier.com/locate/wace

Atmospheric moisture sources associated with extreme precipitation during the peak precipitation month

Marta Vázquez [a,b,c,*], Raquel Nieto [a], Margarida L.R. Liberato [b,c], Luis Gimeno [a]

[a] Environmental Physics Laboratory (EPhysLab), CIM-UVIGO, Universidad de Vigo, Ourense, 32004, Spain
[b] Instituto Dom Luiz, Universidade de Lisboa, 1749-016, Lisboa, Portugal
[c] Escola de Ciências e Tecnologia, Universidade de Trás-os-Montes e Alto Douro, Vila Real, Portugal

ARTICLE INFO

Keywords:
Extreme precipitation
Global moisture sources
Lagrangian analysis

ABSTRACT

Understanding moisture transport is crucial for understanding continental precipitation and extreme precipitation events, which are expected to become substantially more frequent under global warming conditions. In this work, the influence of major global moisture sources on extreme continental precipitation during the peak precipitation month is estimated and compared with climatological patterns. The results show a general change in the pattern of contribution of the primary source of precipitation (the source with the highest contribution) during extreme precipitation events. Most primary sources show a general reduction in their area of influence and a notable reduction in their contribution to the total precipitation.

1. Introduction

Extreme events have been an issue of interest in communities worldwide due to their important socioeconomics impacts. The number of flood events in several regions has risen over recent decades (Paprotny et al., 2018), as have the economic losses associated with these events (EASAC, 2018; Willner et al., 2018); these trends are expected to continue in the future (Roudier et al., 2016). The changes observed in extreme events show geographical variability, with observed increases in heavy precipitation events over most continental areas (IPCC et al., 2013). The effects of extreme precipitation events on society are evident and diverse. Although these events can produce natural disasters such as landslides and floods (Tichavský et al., 2019), which have potentially negative implications for crop yields, migration or energy systems (IPCC et al., 2014), several communities are highly dependent on the occurrence of extreme events for their water resources (Paltan et al., 2017). These uneven implications indicate that it is crucial to better understand the factors that influence the occurrence of extreme events to be able to predict them and allow communities to adapt to their possible consequences.

The effects of global warming have modified global rainfall patterns. However, the changed in observed and expected precipitation show high geographical and temporal variability (Adler et al., 2018; Nguyen et al., 2018; Pendergrass et al., 2017). Associated with higher temperatures, the water holding capacity of the atmosphere increases according to the Clausius-Clapeyron (C–C) relationship, in which the expected increase in water holding capacity is 7% per degree temperature increase (Trenberth et al., 2003). Therefore, an intensification of precipitation is expected. A global mean precipitation pattern cannot be estimated by scaling the C–C relationship; however, extreme precipitation events have a more consistent global relationship (Held and Soden, 2006; Trenberth, 2011). Both observed and predicted extreme events increase under global warming more than mean precipitation (e.g., Myhre et al., 2019; Donat et al., 2016; Papalexiou and Montanari, 2019). For example, according to Myhre et al. (2019), the occurrence of extreme precipitation events would double for each degree of temperature increase if historical trends continue. In general, this behaviour could be caused by the fraction of water vapor converted into rain during such events. During extreme precipitation events, most of the water vapor is precipitated out and, due to the higher moisture availability predicted by the C–C relationship, the upper percentile precipitation is expected to scale with temperature (Allen and Ingram 2002; Pall et al., 2007). However, important latitudinal differences in the response of extreme precipitation events to global warming were observed. These discrepancies are mostly derived from a dynamical contribution (O'Gorman and Schneider, 2009), as vertical motion is significantly relevant to the occurrence of extreme events (Duffy et al., 2020; Li and O'Gorman, 2020).

* Corresponding author. Environmental Physics Laboratory (EPhysLab), CIM-UVIGO, Universidad de Vigo, Ourense, 32004, Spain.
E-mail address: martavazquez@uvigo.es (M. Vázquez).

https://doi.org/10.1016/j.wace.2020.100289
Received 29 June 2020; Received in revised form 15 October 2020; Accepted 5 November 2020
Available online 10 November 2020

Numerous causes have been attributed to the observed changes in recent extreme precipitation events in different areas of the world. At a local scale, the changes in continental land use have been shown to modify precipitation patterns (Allan et al., 2020). In several areas, urbanisation has affected the stability and turbulence of the atmosphere and aerosols derived from pollution have caused changes in cloud microphysics (e.g., Han et al., 2014; Pathirana et al., 2014). Soil moisture also affects convective rainfall by affecting the latent and sensible heating (e.g., Tuttle and Salvucci, 2016; Taylor, 2015). Despite the observed effects of local processes on extreme precipitation changes, many authors have also investigated the effects of atmospheric transport from remote areas. For example, Kunkel et al. (2012) found that the main cause of extreme precipitation events is frontal activity. Volosciuk et al. (2016) suggested that the increase in the Mediterranean Sea temperature amplifies the precipitation extremes over Central Europe during summer. Rising temperatures are expected to produce and intensify areas of evaporation around the world by producing and effecting moisture transport and therefore total and extreme precipitation. Findell et al. (2019) recently found that increasing temperatures produce and intensify the contribution of oceanic evaporation to continental precipitation. The intensity of horizontal moisture transport scales according to the C–C relationship, similar to the relationship shown for extreme precipitation (Held and Soden, 2006; Allan et al., 2020). Therefore, the influence of atmospheric moisture transport on these events is expected to be relevant. Many previous studies have highlighted the influence of moisture transport on global and regional precipitation patterns (e.g., Gimeno et al., 2010; 2020; Viste and Sorteberg, 2013; Hoyos et al., 2018) and, specifically, on the main mechanisms related to precipitation extremes (e.g., Gimeno et al., 2016; Algarra et al., 2019). In addition to the effects of thermodynamic conditions on observed changes in extreme precipitation, the effects of atmospheric circulation also influenced precipitation behaviour at regional scales (Li et al., 2019). As the ocean and continents warm, a change in the evaporation-transport-precipitation relationship is expected; however, the nature of this change remains unclear. In this study, we investigate these relationships by analysing variations in moisture transport from the globally most evaporative regions toward continental areas associated with mean and extreme precipitation. The mean monthly contribution from the main precipitation source to continental areas was previously analysed by Nieto et al. (2019) for intense precipitation months. Their results show that contributions higher than 50% were found over several areas, highlighting the importance of these sources for precipitation in the wet season.

The present study continues the line stablished by Nieto et al. (2019) by selecting only extreme precipitation days from the complete Peak Precipitation Month (PPM) defined in the previous work. The aim of this study is to investigate if there is a different relationship between moisture transport in extreme precipitation events and that in mean precipitation during the peak precipitation month. Therefore, we analyse the influence of the main global evaporative regions defined in Gimeno et al. (2010) on extreme precipitation events by employing widely used Lagrangian techniques for moisture transport analysis, and by comparing the results with those observed at a climatological scale by Nieto et al. (2019).

2. Methodology

2.1. Peak precipitation month definition

The Peak Precipitation Month (PPM) is used to select the periods of maximum precipitation. The PPM is the month that shows the highest climatological precipitation value, and in this analysis, it was computed using daily precipitation data from the CPC Global Unified Gauge-Based Analysis of Daily Precipitation (Chen et al., 2008) provided by the NOAA/OAR/ESRL Physical Science Division with 0.5° horizontal resolution for the period 1980–2018. To find the PPM, the monthly total precipitation is computed by adding the daily precipitation values at every grid point following Nieto et al. (2019); finally, the PPM is selected as the month that shows the highest total monthly precipitation value. The resulting PPMs are presented in Fig. 1. In general, the distribution is similar to that found in Nieto et al. (2019), which was calculated using the MSWEP database (Beck et al., 2017).

2.2. Moisture sources definition

The monthly moisture sources were computed for the period 1980–2015 following the methodology established by Gimeno et al. (2010), using Vertically Integrated Moisture Flux (VIMF) divergence. Continental and oceanic moisture sources were defined monthly and 40 and 50 percentile thresholds of the VIMF divergence, respectively, were used to delimitate them. Fourteen sources were defined, namely the North Pacific (NPAC), South Pacific (SPAC), Gulf of Mexico and Caribbean Sea (MEXCAR), North Atlantic (NATL), South Atlantic (SATL), Zanzibar Current and Arabian Sea (ZANAR), Agulhas Current (AGU), Indian Ocean (IND), Coral Sea (CORALS), Mediterranean Sea (MED), Red Sea (REDS), South America (SAM), Sahel region (SAHEL), and Southern Africa (SAFR). Fig. 2 shows these sources for the month with the highest area. Further details about the computation and the specific threshold values used for every source can be found in Nieto et al. (2019).

2.3. Moisture transport analysis

To compute moisture transport, the Lagrangian particle dispersion model FLEXPART v9.0 (Stohl et al., 1998, 2005; Stohl and Thomson, 1999; Pisso et al., 2019) and the methodology establish by Stohl and James (2004, 2005) were used. The model is fed by the ECMWF ERA-Interim reanalysis data at 1° horizontal resolution, which allows the trajectories of a high number of air particles to be followed and the changes in several variables along their paths to be analysed. In the present experiment, a total of approximately 2 million particles are homogeneously globally distributed and dispersed following the 3D wind fields. To compute the moisture changes, the position and specific humidity (q) of every individual particle is stored with a 6 h temporal resolution.

In the present analysis, the particles initially located over every individual moisture source are selected and tracked forward in time. The moisture changes experienced by the particles between two time steps (dt) along their paths from the moisture sources can be estimated following the equation $e - p = m\, dq/dt$, where e and p represent the moisture increase and decrease, respectively, experienced by the particle, and m its mass. Considering the (e-p) contribution from all particles at every grid position, the total surface freshwater flux can be computed as $E - P = \frac{\sum_{k=1}^{K}(e-p)}{A}$, where E and P are the evaporation and precipitation per unit area, respectively, A is the area of the grid cell and K is the total number of particles at every grid column. A schematic representation of the procedure in the E-P computation is presented in Fig. 3. Over the regions where $E - P < 0$, the particles lose moisture, and therefore areas in which the source contributes moisture for precipitation is estimated as $|E - P < 0|$.

To investigate the moisture contribution from every source associated with extreme precipitation events in the PPM a composite analysis was performed that considers the days with precipitation above the 95th percentile of wet days (those days with precipitation higher than 1 mm) for the period 1980–2018. This selection was performed for every grid point using CPC daily precipitation data with a 0.5 × 0.5 horizontal resolution.

To compute the moisture contribution from every source for the extreme precipitation days over each grid point, the air particles were followed in forward mode along their paths during the optimal time as indicated in Nieto and Gimeno (2019). The database presented by Nieto

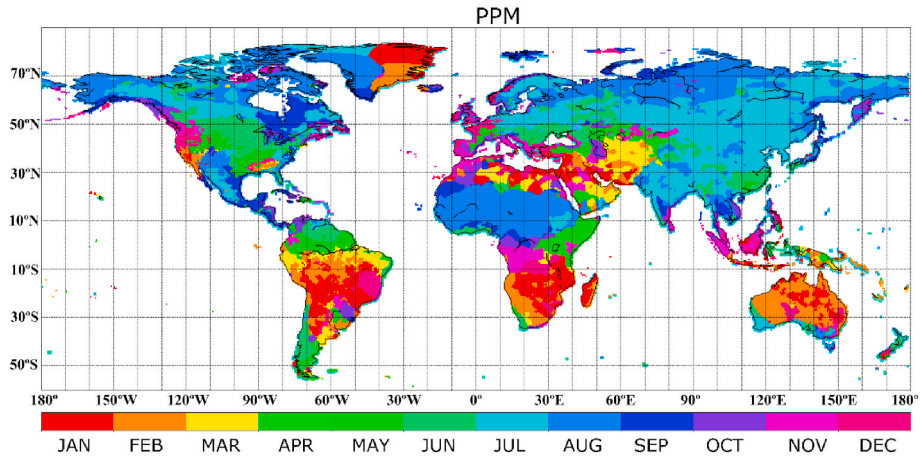

Fig. 1. Month of maximum precipitation (PPM) for every grid point computed from CPC daily data for the period 1980–2018.

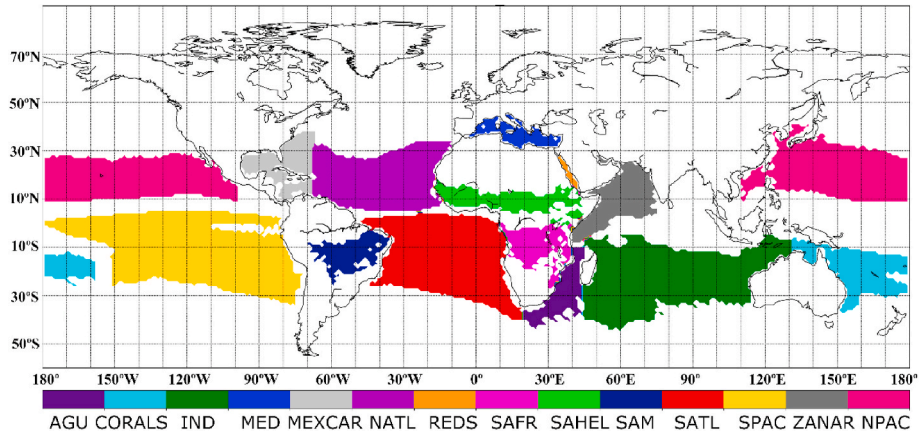

Fig. 2. Moisture sources in the month of maximum source area.

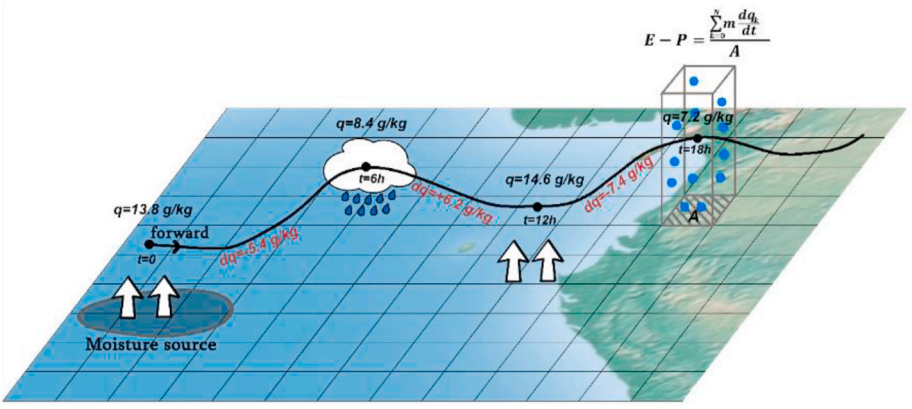

Fig. 3. Schematic representation of the moisture transport analysis procedure. The black line and dots represent the trajectory of a single particle. The vertical arrows represent the areas of moisture uptake where $dq > 0$ by surface evaporation and the cloud represents a loss of moisture by precipitation ($dq < 0$). The gray vertical box represents an atmospheric column over which dq from all the particles residing within it are summed to obtain the total $E - P$.

and Gimeno (2019) provide the optimal integration times for Lagrangian studies of source-sink relationships, which are available at a 0.25° horizontal resolution for every grid parcel. It is expected that most of the moisture contributed to a specific region would take a maximum time equal to the optimum time to be transported from all the possible sources. Moreover, not all particles that leave the moisture source would travel at the same velocity and the time taken to reach a specific area would vary from one region to another. For this reason, if an extreme precipitation event occurs on a specific day over a grid area and if, for example, the optimal time is 10 days, then the moisture that arrives on that day contributes to precipitation that could have left a specific moisture source from 1 to 10 days before the extreme precipitation occurred. Therefore, in this experiment, the total moisture contribution associated with every extreme precipitation event is computed at every

grid parcel and the transport time, which ranges from 1 to t_{opt} days (being t_{opt} the optimal time for that specific grid parcel) is taken into account.

3. Results and discussion

3.1. Moisture sources associated with extreme precipitation

Taking into consideration the total contribution from all moisture sources over every grid point for the PPMs and their extreme precipitation events, the preferred (higher moisture contribution) and secondary moisture sources are computed following the methodology described in Nieto el al. (2019).

At every grid point all sources that show some amount of moisture contribution are considered to influence the precipitation over each point. Fig. 4 shows the total number of sources of moisture by grid point for the climatological precipitation in the PPM and for the extreme events in the PPM. High spatial variability is observed in both cases. In the PPM climatology, less than 7 sources influence the precipitation in most of the grids. The northern regions show a lower number of moisture sources; western Central Africa shows the maximum. During extreme events, the distribution of the sources shows important

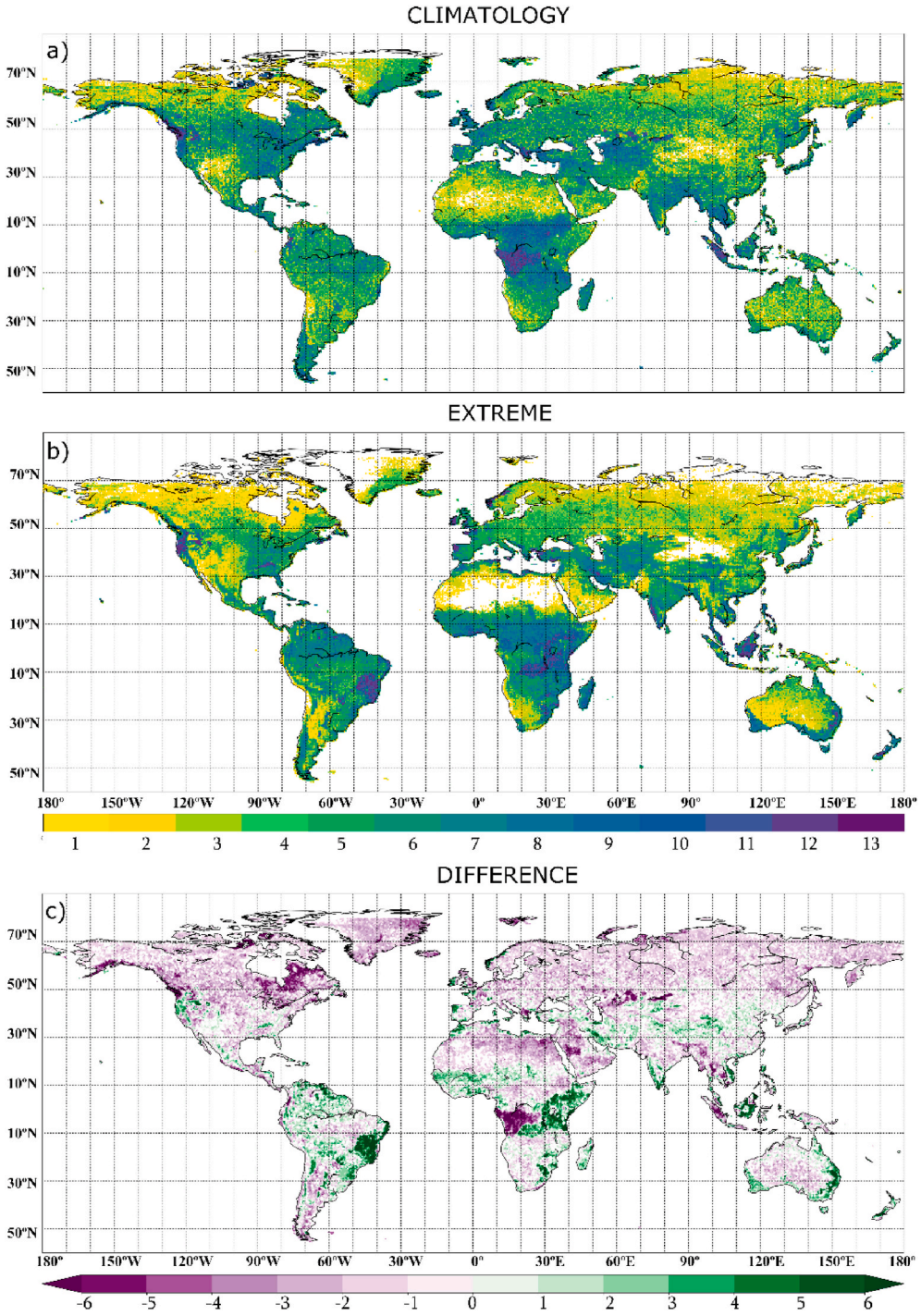

Fig. 4. Number of moisture sources by grid that contribute to the precipitation for (a) the PPM climatology, for (b) the extreme precipitation events, and for (c) the difference between these.

variations compared with those of the PPM climatology. The number of sources significantly decreases over most of Eurasia and Western North America, being this reduction higher over eastern Canada. The only exceptions occur over some western coastal areas in both continents. Similar behaviour can be observed in Australia, where a decrease in the number of sources is observed in the center of the country, but not along the coast. The major differences in the number of moisture sources can be observed in parts of Brazil, South America, in northeastern North America, and over central Africa.

Fig. 5 shows how the main source over every region influences extreme precipitation. On this Figure the upper panel (Fig. 5a) shows the preferred moisture source (PS) computed by considering all the days of the PPM, which is hereinafter referred to as the climatological PS. In Fig. 5b, the PS changes in the extreme precipitation days (areas with no colour, which have the same PS as in Fig. 5a) are plotted. However, to demonstrate a general pattern of the PSs for the extreme events, a complete map is presented in the supplementary material (Fig. S1a). Changes in the PS occur over important areas all over the world, at approximately 30%.

Over most of **North America**, the PS was associated with extreme events is the North Pacific source. Compared to the climatological values, the NPAC source increased its area of influence eastward and northward, supplying the NATL and MEXCAR with climatological influence.

Over **South America**, the four main climatological sources (NATL, SATL, SPAC and SAM) are also identified as preferred sources for the extreme events. However, the SPAC shows a northward and eastward expansion of its area of influence, retracting the limits of NATL and SATL. Over most of Brazil the influence of NATL does not change compared to that of the PPM climatology; however, over the southern area, the SATL source gains importance.

In **Africa**, the PS that affects a higher area is the SATL source in both PPM climatology and extreme precipitation in the PPM. However, the influence of this source shows a southward expansion associated with extreme events. Over South Africa, the increased influence of SATL sources reduces the extension of the area affected by the AGU source, which is situated to the east of the continent. In eastern Africa, over the Horn of Africa, the IND contribution area decreased as the ZANAR increased, associated with extreme events. The area affected by the continental SAFR source showed a southwestward shift for the extreme events, and the REDS source showed a higher influence westward, over the eastern Sahel region. Finally, the SAHEL continues as the PS over the Congo region.

In **Eurasia,** five main sources appear to be associated with climatological precipitation in the PPM, namely the NATL, MED, ZANAR, NPAC and REDS sources, and all of these appear to be associated with extreme

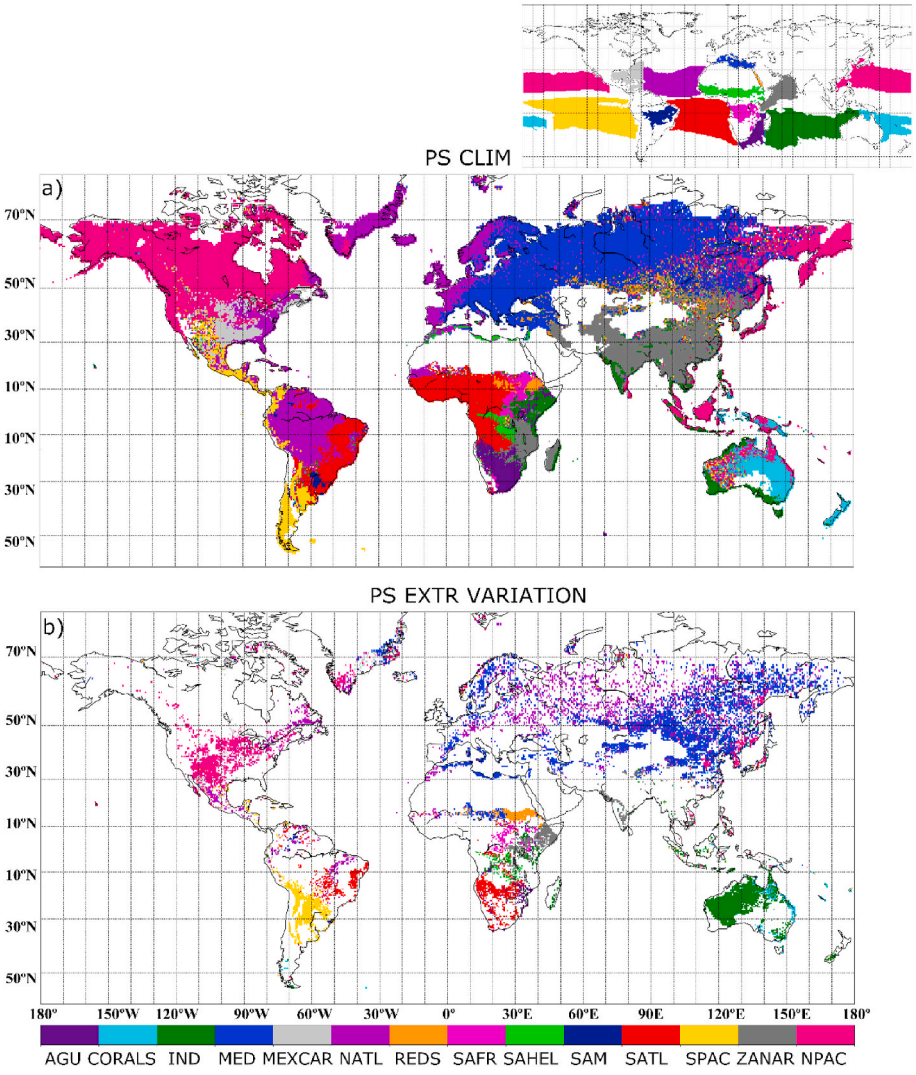

Fig. 5. (a) Gridded Preferred Source (PS) for the PPM for all days. (b) Areas where the PS for extreme precipitation events in the PPM changed compared to that in (a).

precipitation (Fig. 5 and S1a). The MED and NATL sources are dominant and their influence increased in the extreme events; it is especially evident in the increase in the area of influence of MED. This source gained special relevance over East Asia, expanding its influence further south, and its influence also increased over the Scandinavian peninsula and around the MED source itself.

Finally, over **Australia**, the IND source gained a relevant importance for extreme precipitation, weakening the role of the SPAC.

In most of the continents an increase in the expansion of the sources westward of the sink was observed. This is the case for the NPAC over North America, NATL and MED over Eurasia, SATL over South Africa, SPAC over South America or IND over Australia.

The secondary and tertiary sources are also important; they are represented in Fig. S2 in Supplementary Material, in the same way as in Fig. 5. In general, the climatological patterns of both PSs are more uneven. In the case of the secondary sources over **Eurasia,** the influences of MED and NATL were observed in the redistribution relative to the PPM climatology. Both figures (Fig. 5 and S2a) and the tertiary source (Fig. S2b) show that the trajectories of the meteorological systems that transport moisture from these sources move further to the south and to the east than in the PPM climatology. Over **North America**, the observed increase in the area of influence of NPAC as the PS to the east also continues when it acts as a secondary and tertiary source. Moreover, over Alaska and northwestern regions, the area of influence from the MED significantly increases. However, as expected, the contribution from this source over this area is very low (see Fig. S3). Mediterranean particles reach those areas, in addition to the eastward expansion of the NPAC in determining the MEXCAR or NATL, suggesting that the extreme events over this part of the continent are mostly associated with the addition of moisture from the west.

In **South America**, the SATL and SPAC sources show a northwestward and northeastward expansion of their area of influence, respectively, associated with their acting as secondary and tertiary sources for extreme events. The expansion of these sources for the three orders of the PS (primary, secondary, and tertiary) commonly affected areas where NATL showed a high impact at the climatological scale.

Finally, over **Africa**, a change in the secondary and tertiary source was observed over most of the area. However, **only** the SATL increased its influence over South America and can be extracted from the results (associated with the PS and secondary source).

To provide a synthesis at the global scale for the change in the order of importance of each source, Table 1 shows the total area influenced by every source at different impact levels (PS, secondary, tertiary, and all the remaining sources) for the PPM climatology and extreme events days. Blue (red) colours in this table represent those levels in which the total area of influence for the source decreased (increased) associated with extreme events. Overall, most of the sources decreased their area of influence. When analysing the influence of every source as the PS at a global scale, only the MED and IND show an increase. The area of influence of the MED was associated with extreme events and is higher at all levels of influence, especially as a secondary source. In the case of NATL, the area of influence increases at all levels with the exception of the PS. In general, it is important to notice that the total area of this source highly decreases as the level of influence increases.

Table 1
Total continental area (expressed in units x 10^7 km^2) affected by each moisture source at a different level of influence for PPM climatological values and for the extreme events. Blue (red) colours on right hand table represent decrease (increase) in the total continental area in extreme events compared with climatological value.

	CLIM				EXTR			
	PS	2º	3º	4º	PS	2º	3º	4º
AGU	7,40	0,75	1,13	4,83	4,50	0,72	1,07	3,29
CORALS	11,02	0,94	0,75	4,70	7,23	0,93	0,38	2,24
IND	13,69	2,72	1,76	4,73	16,67	2,31	1,08	3,29
MED	40,65	1,65	1,23	3,87	50,59	2,82	1,56	4,24
MEXCAR	7,27	1,66	1,55	3,43	5,66	1,22	1,18	4,46
NATL	40,76	4,90	1,95	2,88	37,72	5,39	2,31	3,61
REDS	9,99	2,10	2,08	4,70	7,45	0,86	1,65	4,29
SAFR	4,01	0,74	1,12	2,30	3,03	0,57	0,51	1,94
SAHEL	5,61	1,56	2,11	2,44	2,34	0,64	0,88	2,97
SAM	1,39	0,44	0,73	1,95	0,84	0,22	0,55	0,9
SATL	30,38	2,27	1,59	4,13	27,68	2,16	1,21	2,78
SPAC	12,94	1,46	1,81	4,72	12,53	1,11	1,39	3,77
ZANAR	40,06	1,89	1,84	4,93	33,70	1,30	1,37	3,67
NPAC	43,35	1,83	1,96	3,52	39,37	1,20	2,55	4,46

3.2. *Contribution of the moisture sources to extreme precipitation*

Fig. 6 shows the percentage of contribution for extreme precipitation events provided by the PS and the difference with the percentage of climatological values. The total PS contributions for the PPM climatology and extreme precipitation days (Fig. S4) as well as PPM climatology total percentage contribution to precipitation (Fig. S5) are presented in Supplementary material. The higher percentage of contribution by the PS associated with extreme precipitation events are over the North America, eastern South America, southern Europe and around Mediterranean Sea, Indian peninsula, eastern Africa, and western areas of Africa closest to the Gulf of Guinea. These areas are similar to those showing higher contribution percentage on the climatological analysis. However, reductions higher than 10% appears for the extreme precipitation over most of them (Fig. 6b), with the exception for NE Brazil. It is important to note that, as expected, the total contribution from the PS highly increase associated with extreme events (Fig. S4). However, the relative importance of the sources is the aim of this section. Some significant increase in percentage is observed over areas of western USA associated with NPAC source, or eastern and central South America where SPAC is the PS (Fig. S1). Over western Australia, an increment on the moisture contribution percentage is observed associated with extreme precipitation; in this case the PS varies from the CORAL and NPAC in the PPM climatology (Fig. 5a) to IND during extreme precipitation events (Fig. 5b).

Western USA, Europe, and several regions of southern Asia have higher percentages of contributions, explained by the secondary source (Fig. S3a, left column). This suggests that these areas are the most influenced by the main global moisture sources, not only for extreme events but also for the PPM climatology (see Fig. S5). The specific moisture sources with higher impacts in both cases for every specific area are the NPAC and MEXCAR over USA, MED and NATL over western Europe, and IND and ZANAR over southern Asia (see Fig. S1, 5 and S2a). However, both sources are the two most important in the extreme events and PPM climatology, their order of importance varies in several of these areas. In general, areas of higher contribution show higher reductions in extremes relative to the contribution for the PS (Fig. 6); however, the situation with the secondary source is not clear (Fig. S3a, right column). For example, an important increase in the percentage of precipitation explained for the NATL (when acting as secondary source) is observed over Europe (see Fig. S1a). Other areas that show an increase in the percentage of the moisture contribution to precipitation are southern Africa, several regions of central and eastern South America, or Australia. These increases were also observed in the PS over closest areas and related with the same sources namely SATL, SPAC and IND; confirming the increased influence of this sources on extreme precipitation patterns over those areas.

In contrast with this increased influence, reductions in the percentage of the moisture contribution was attributed to the PS and a secondary source associated with extreme events was observed over northeastern Brazil, central and eastern Africa, and eastern North America.

Finally, in the sources acting as a tertiary source, the total percentage of the moisture contribution associated with extreme events highly decreases (Fig. S3b, left column), and the differences with the PPM

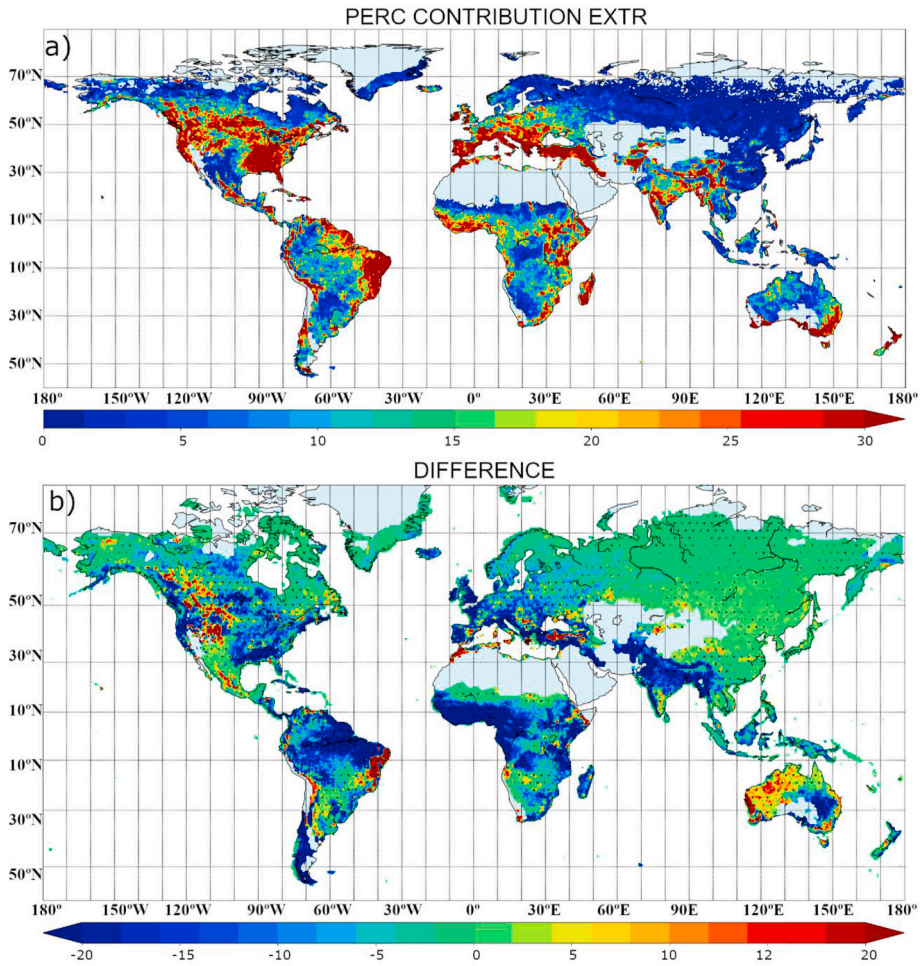

Fig. 6. a) Percentage of contribution from the PS for extreme events. b) Difference between the percentage observed in a) and PPM climatology. Dots represent significant differences at 95%.

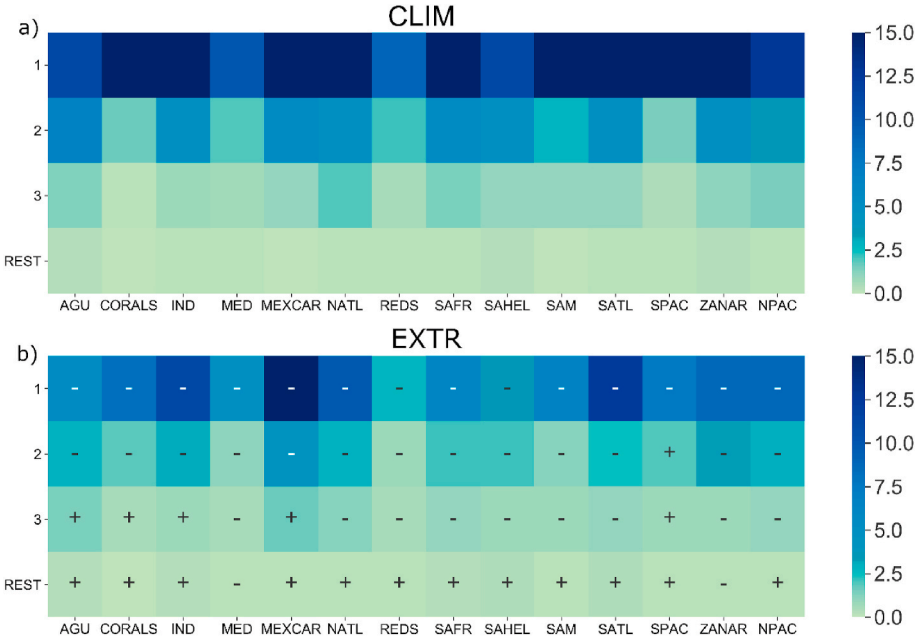

Fig. 7. Global moisture contribution percentage of every source associated with a) total PPM and b) extreme events. The horizontal axis in both figures represents the level of influence of every source.

climatology do not show, in general, important variation.

To investigate the individual behaviour of the sources, Fig. 7 shows the moisture contribution percentage calculated for the total global area where each source acts as a PS, and also at lower levels of influence (vertical axis in the Figure). This is computed for the climatological moisture contribution (Fig. 7a) and for the value associated with extreme precipitation (Fig. 7b). In Fig. 7b the symbols within the cells describe the variation in the percentage of extreme events compared with that of the PPM climatology. Therefore, the plus ("+") sign represents those influence levels where the percentage of contribution increases for extreme events, and the minus ("-") sign indicates the opposite. The REST row (last row in Fig. 7a and b) describes the combined contribution from sources 4 to 14 in importance. On this Figure only the main global moisture sources described in Fig. 2 are included, so the percentage of contribution not accounted should be associated to local sources, not considered in the present study.

For the PS, all sources reduce their percentage for the extreme precipitation events compared with those of the climatological value. The same is true for secondary sources, with the exception of SPAC. The number of sources that increase the percentage grows, when they act as tertiary sources, to five; and this number increases as the level of influence of the source decreases (result not shown). One source that deserves particular attention is the SPAC, which increases over most of the levels; however, its global area of influence decreases at most of the levels (see Table 1). This could be explained by the fact that, despite a decrease in its area of influence over other areas, such as North America, a significant increase is observed over Southern America, and the new areas of influence are associated with an increase in the percentage of contribution (see Figs. S1 and S2 vs Fig. 6 and S3). In the case of, for example, the MED contribution, the situation is different. This source appears to increase the area with influence in precipitation since this increase is observed at all levels (see Table 1). However, its global percentage of contribution decreases for most of the levels (more than 70%). There is not a clear increase in the moisture contribution percentage from this source observed in any region at the higher influence levels (preferred, secondary, and tertiary source) (see Fig. 6 and S3). In contrast, a higher influence on precipitation extreme is observed, for example, over Europe from NATL, despite MED being the PS over most of the area (Fig. 6 and S3).

4. Conclusions

In this work, a Lagrangian approach was used to compare extremes versus climate related moisture transport from the main global moisture sources towards the continents during the peak precipitation month.

The area of influence of the main moisture source showed a general redistribution when associated with extreme events. At a global scale, most of the sources showed a reduction in the total area of influence, with the exception of MED and NATL, which increased their area of influence further east over Eurasia, while the SPAC increased over central South America, SATL increased over South Africa and the IND increased over Australia.

The contribution of the sources to the total precipitation also showed a notable reduction in extreme events versus those related to PPM climatology, with reductions in the primary sources higher than 10% over most of the continental areas. This reduction decreases as the level of influence of the sources decreases. There were no exceptions as the changes in the percentage of contribution for extreme events observed over western USA, eastern and central South America and Australia were associated the NPAC, SPAC and IND sources, respectively, when these sources acting as a primary source.

These three sources and NATL and MED extend their influence to the east when the extreme events are studied; this favoured flow could be related to a specific dynamical condition, since modes of climate variability modify the moisture transport, which should be investigated further in the future.

Our analysis only considered main global moisture sources. The analysis suggests that other sources of moisture not investigated here are highly important sources for extreme precipitation. In particular, local processes, such as recycling, or regional sources could have an important effect and should be investigated in future analyses. The present study is intended as the starting point for other regional analysis in which different sources contribution and/or general wet spells (not necessarily based on the PPM) could be investigated; as well as the mechanisms associated with these events and their variability. Specifically, the analysis of teleconnection pattern result of special interest taking into consideration their effect on regional precipitation patterns. Moreover, synoptic analysis could be relevant over some regions such as the Europe, in order to investigate the observed MED to NATL shift associated with extreme events.

CRediT authorship contribution statement

Marta Vázquez: Conceptualization, Methodology, Software, Visualization, Investigation, Formal analysis, Writing - original draft, Writing - review & editing. **Raquel Nieto:** Conceptualization, Supervision, Funding acquisition, Methodology, Writing - review & editing. **Margarida L.R. Liberato:** Supervision, Methodology, Formal analysis, Writing - review & editing. **Luis Gimeno:** Supervision, Conceptualization, Funding acquisition, Writing - review & editing.

Declaration of competing interest

The authors declare that they have no known competing financial interests or personal relationships that could have appeared to influence the work reported in this paper.

Acknowledgements

This work forms part of the LAGRIMA project (RTI2018-095772-B-I0O) funded by Ministerio de Ciencia, Innovación y Universidades. Marta Vazquez is supported by the Xunta de Galicia under grant ED481B 2018/062. Margarida L.R. Liberato acknowledges funding from Fundação para a Ciência e a Tecnologia, Portugal (FCT) and Portugal Horizon 2020 through project WEx-Atlantic (PTDC/CTA-MET/29,233/2017) and for the academic mobility to the Environmental Physics Laboratory (EPhysLab), Universidade de Vigo, Spain under Fundación Carolina (C.2019). This work was partially supported by Xunta de Galicia under Project ED431C 2017/64-GRC "Programa de Consolidación e Estructuración de Unidades de Investigación Competitivas (Grupos de Referencia Competitiva)".

Appendix A. Supplementary data

Supplementary data to this article can be found online at https://doi.org/10.1016/j.wace.2020.100289.

References

Adler, R., Sapiano, M., Huffman, G., Wang, J.–J., Gu, G., Bolvin, D., Chiu, L., Schneider, U., Becker, A., Nelkin, E., Xie, P., Ferraro, R., Shin, D.B., 2018. The global precipitation climatology project (GPCP) monthly analysis (new version 2.3) and a review of 2017 global precipitation. Atmosphere 9 (4), 138. https://doi.org/10.3390/atmos9040138.

Algarra, I., Eiras-Barca, J., Miguez-Macho, G., Nieto, R., Gimeno, L., 2019. On the assessment of the moisture transport by the Great Plains low-level jet. Earth Syst. Dynam. 10, 107–119. https://doi.org/10.5194/esd-10-107-2019, 2019.

Allan, R.P., Barlow, M., Byrne, M.P., Cherchi, A., Douville, H., Fowler, H.J., Gan, T.Y., Pendergrass, A.G., Rosenfeld, D., Swann, A.L.S., Wilcox, L.J., Zolina, O., 2020. Advances in understanding large-scale responses of the water cycle to climate change [published online ahead of print]. Ann. N. Y. Acad. Sci. https://doi.org/10.1111/nyas.14337, 2020, 10.1111/nyas.14337.

Allen, M., Ingram, W., 2002. Constraints on future changes in climate and the hydrologic cycle. Nature 419, 228–232. https://doi.org/10.1038/nature01092.

Beck, H.E., van Dijk, A.I., Levizzan, V., Schellekens, J., Gonzalez Miralles, D., Martens, B., de Roo, A., 2017. MSWEP: 3-hourly 0.25° global gridded precipitation

(1979-2015) by merging gauge, satellite, and reanalysis data. Hydrol. Earth Syst. Sci. 21 (1), 589–615. https://doi.org/10.5194/hess-21-589-2017.
Chen, M., Shi, W., Xie, P., Silva, V.B.S., Kousky, V.E., Higgins, R.W., Janowiak, J.E., 2008. Assessing objective techniques for gauge-based analyses of global daily precipitation. J. Geophys. Res. 113, D04110. https://doi.org/10.1029/2007JD009132.
Donat, M., Lowry, A., Alexander, L.V., O'Gorman, P.A., Maher, N., 2016. More extreme precipitation in the world's dry and wet regions. Nat. Clim. Change 6, 508–513. https://doi.org/10.1038/nclimate2941.
Duffy, M.L., O'Gorman, P.A., Back, L.E., 2020. Importance of laplacian of low-level warming for the response of precipitation to climate change over tropical oceans. J. Clim. 33 (10), 4403–4417. https://doi.org/10.1175/jcli-d-19-0365.1.
European Academies' Science Advisory Council, 2018. Extreme Weather Events in Europe. EASAC. Report No. 22. https://easac.eu/publications/details/extreme-weather-events-in-europe/.
Findell, K.L., Keys, P.W., van der Ent, R.J., Lintner, B.R., Berg, A., Krasting, J.P., 2019. Rising temperatures increase importance of oceanic evaporation as a source for continental precipitation. J. Clim. 32, 7713–7726. https://doi.org/10.1175/JCLI-D-19-0145.1.
Gimeno, L., Dominguez, F., Nieto, R., Trigo, R., Drumond, A., Reason, C.J.C., Taschetto, A.S., Ramos, A.M., Kumar, V., Marengo, J., 2016. Major mechanisms of atmospheric moisture transport and their role in extreme precipitation events. Annu. Rev. Environ. Resour. 41 (1), 117–141. https://doi.org/10.1146/annurev-environ-110615-085558.
Gimeno, L., Drumond, A., Nieto, R., Trigo, R.M., Stohl, A., 2010. On the origin of continental precipitation. Geophys. Res. Lett. 37, L13804. https://doi.org/10.1029/2010GL043712.
Gimeno, L., Vázquez, M., Eiras-Barca, J., Sorí, R., Stojanovic, M., Algarra, I., Nieto, R., Ramos, A.M., Durán-Quesada, A.M., Dominguez, F., 2020. Recent progress on the sources of continental precipitation as revealed by moisture transport analysis. Earth Sci. Rev. 201 (103070), 1–25. https://doi.org/10.1016/j.earscirev.2019.103070.
Han, J., Baik, J., Lee, H., 2014. Urban impacts on precipitation. Asia-Pacific. J. Atmos. Sci. 50, 17–30. https://doi.org/10.1007/s13143-014-0016-7.
Held, I.M., Soden, B.J., 2006. Robust responses of the hydrological cycle to global warming. J. Clim. 19 (21), 5686–5699. https://doi.org/10.1175/JCLI3990.1.
Hoyos, I., Dominguez, F., Cañón-Barriga, J., Martínez, A.A., Nieto, R., Gimeno, L., Dirmeyer, P.A., 2018. Moisture origin and transport processes in Colombia, northern South America. Clim. Dynam. 50, 971–990. https://doi.org/10.1007/s00382-017-3653-6.
IPCC, 2013. In: Stocker, T.F., Qin, D., Plattner, G.-K., Tignor, M., Allen, S.K., Boschung, J., Nauels, A., Xia, Y., Bex, V., Midgley, P.M. (Eds.), Climate Change 2013: the Physical Science Basis. Contribution of Working Group I to the Fifth Assessment Report of the Intergovernmental Panel on Climate Change. Cambridge University Press, Cambridge, United Kingdom and New York, NY, USA, 1535 pp.
IPCC, 2014. In: Field, C.B., Barros, V.R., Dokken, D.J., Mach, K.J., Mastrandrea, M.D., Bilir, T.E., Chatterjee, M., Ebi, K.L., Estrada, Y.O., Genova, R.C., Girma, B., Kissel, E. S., Levy, A.N., MacCracken, S., Mastrandrea, P.R., White, L.L. (Eds.), Climate Change 2014: Impacts, Adaptation, and Vulnerability. Part A: Global and Sectoral Aspects. Contribution of Working Group II to the Fifth Assessment Report of the Intergovernmental Panel on Climate Change. Cambridge University Press, Cambridge, United Kingdom and New York, NY, USA, 1132 pp.
Kunkel, K.E., Easterling, D.R., Kristovich, D.A., Gleason, B., Stoecker, L., Smith, R., 2012. Meteorological causes of the secular variations in observed extreme precipitation events for the conterminous United States. J. Hydrometeorol. 13, 1131–1141. https://doi.org/10.1175/JHM-D-11-0108.1.
Li, C., Zwiers, F., Zhang, X., Chen, G., L, J., Li, G., Norris, J., Tan, Y., Sun, Y., Liu, M., 2019. Larger increases in more extreme local precipitation events as climate warms. Geophys. Res. Lett. 46, 6885–6891. https://doi.org/10.1029/2019GL082908.
Li, Z., O'Gorman, P., 2020. Response of vertical velocities in extratropical precipitation extremes to climate change. J. Clim. https://doi.org/10.1175/JCLI-D-19-0766.1.
Myhre, G., Alterskjær, K., Stjern, C.W., Hognebrog, O., Marelle, L., Samset, B.H., Sillmann, J., Schaller, N., Fisher, E., Schulz, M., Stohl, A., 2019. Frequency of extreme precipitation increases extensively with event rareness under global warming. Sci. Rep. 9, 1606. https://doi.org/10.1038/s41598-019-52277-4.
Nguyen, P., Thorstensen, A., Sorooshian, S., Hsu, K., Aghakouchak, A., Ashouri, H., Tran, H., Braithwaite, D., 2018. Global precipitation trends across spatial scales using satellite observations. Bull. Am. Meteorol. Soc. 99, 689–697. https://doi.org/10.1175/BAMS-D-17-0065.1.
Nieto, R., Gimeno, L., 2019. A database of optimal integration times for Lagrangian studies of atmospheric moisture sources and sinks. Scientific Data 6, 1–10. https://doi.org/10.1038/s41597-019-0068-8.
Nieto, R., Ciric, D., Vázquez, M., Liberato, M.L.R., Gimeno, L., 2019. Contribution of the main moisture sources to precipitation during extreme peak precipitation months. Adv. Water Resour. 131, 1–8. https://doi.org/10.1016/j.advwatres.2019.103385.
O'Gorman, P.A., Schneider, T., 2009. The physical basis for increases in precipitation extremes in simulations of 21st-century climate change. Proc. Natl. Acad. Sci. U. S. A. 106 (35), 14773–14777. https://doi.org/10.1073/pnas.0907610106.
Pall, P., Allen, M.R., Stone, D.A., 2007. Testing the Clausius–Clapeyron constraint on changes in extreme precipitation under CO_2 warming. Clim. Dynam. 28, 351–363. https://doi.org/10.1007/s00382-006-0180-2.
Paltan, H., Waliser, D., Lim, W.H., Guan, B., Yamazaki, D., Pant, R., Dadson, S., 2017. Global floods and water availability driven by atmospheric rivers. Geophys. Res. Lett. 44 (10), 395. https://doi.org/10.1002/2017GL074882, 387– 10.
Papalexiou, S.M., Montanari, A., 2019. Global and regional increase of precipitation extremes under global warming. Water Resour. Res. 55, 4901–4914. https://doi.org/10.1029/2018WR024067.
Paprotny, D., Sebastian, A., Morales-Nápoles, O., Jonkman, S.N., 2018. Trends in flood losses in Europe over the past 150 years. Nat. Commun. 9, 1985. https://doi.org/10.1038/s41467-018-04253-1.
Pathirana, A., Denekew, H.B., Veerbeek, W., Zevenbergen, C., Banda, A.T., 2014. Impact of urban growth-driven landuse change on microclimate and extreme precipitation - a sensitivity study. Atmos. Res. 138, 59–72. https://doi.org/10.1016/j.atmosres.2013.10.005.
Pendergrass, A.G., Knutti, R., Lehner, F., Deser, C., Sanderson, B.M., 2017. Precipitation variability increases in a warmer climate. Sci. Rep. 7, 17966. https://doi.org/10.1038/s41598-017-17966-y.
Pisso, I., Sollum, E., Grythe, H., Kristiansen, N., Cassiani, M., Eckhardt, S., Arnold, D., Morton, D., Thompson, R.L., Zwaaftink, C.D.G., Evangeliou, N., Sodemann, H., Haimberger, L., Henne, S., Brunner, D., Burkhart, J.F., Fouilloux, A., Brioude, J., Philipp A, M. Seibert P., Stohl, A., 2019. The Lagrangian particle dispersion model FLEXPART version 10.3. Geosci. Model Dev. Discuss. (GMDD) 1–67. https://doi.org/10.5194/gmd-2018-333.
Roudier, P., Andersson, J.C.M., Donnelly, C., Feyen, L., Greuell, W., Ludwig, F., 2016. Projections of future floods and hydrological droughts in Europe under a +2°C global warming. Climatic Change 135, 341–355. https://doi.org/10.1007/s10584-015-1570-4.
Stohl, A., Hittenberger, M., Wotawa, G., 1998. Validation of the Lagrangian particle dispersion model FLEXPART against large scale tracer experiments. Atmos. Environ. 32, 4245–4264. https://doi.org/10.1016/S1352-2310(98)00184-8.
Stohl, A., Thomson, D.J., 1999. A density correction for Lagrangian particle dispersion models. Bound.-Layer Met. 90, 155–167. https://doi.org/10.1023/A:1001741110696.
Stohl, A., Forster, C., Frank, A., Seibert, P., Wotawa, G., 2005. Technical note: the Lagrangian particle dispersion model FLEXPART version 6.2. Atmos. Chem. Phys. 5, 2461–2474. https://doi.org/10.5194/acp-5-2461-2005.
Stohl, A., James, P.A., 2004. A Lagrangian analysis of the atmospheric branch of the GlobalWater cycle. Part I: method description, validation, and demonstration for the August 2002 flooding in central Europe. J. Hydrometeorol. 5, 656–678. https://doi.org/10.1175/1525-7541(2004)005<0656:ALAOTA>2.0.CO;2.
Stohl, A., James, P.A., 2005. A Lagrangian analysis of the atmospheric branch of the GlobalWater cycle. Part II: moisture transports between earth's ocean basins and river catchments. J. Hydrometeorol. 6, 961–984. https://doi.org/10.1175/JHM470.1.
Taylor, C.M., 2015. Detecting soilmoisture impacts on convective initiation in Europe. Geophys. Res. Lett. 42, 4631–4638. https://doi.org/10.1002/2015GL064030.
Tichavský, R., Ballesteros-Cánovas, J.A., Šilhán, K., Tolasz, R., Stoffel, M., 2019. Dry spells and extreme precipitation are the main trigger of landslides in central Europe. Sci. Rep. 9, 14560. https://doi.org/10.1038/s41598-019-51148-2.
Trenberth, K.E., 2011. Changes in precipitation with climate change. Clim. Res. 47, 123–138. https://doi.org/10.3354/cr00953.
Trenberth, K.E., Dai, A., Rasmussen, R.M., Parsons, D.B., 2003. The changing character of precipitation. Bull. Am. Meteorol. Soc. 84, 1205–1217. https://doi.org/10.1175/BAMS-84-9-1205.
Tuttle, S., Salvucci, G., 2016. Empirical evidence of contrasting soil moisture–precipitation feedbacks across the United States. Science 352 (6287), 825–828. https://doi.org/10.1126/science.aaa7185.
Viste, E., Sorteberg, A., 2013. The effect of moisture transport variability on Ethiopian summer precipitation. Int. J. Climatol. 33, 3106–3123. https://doi.org/10.1002/joc.3566.
Volosciuk, C., Maraun, D., Semenov, V., Tilinina, N., Gulev, S.K., Latif, M., 2016. Rising Mediterranean Sea surface temperatures amplify extreme summer precipitation in central Europe. Sci. Rep. 6, 32450. https://doi.org/10.1038/srep32450.
Willner, S.N., Otto, C., Levermann, A., 2018. Global economic response to river floods. Nat. Clim. Change 8, 594–598. https://doi.org/10.1038/s41558-018-0173-2.